Petroleum Science 20 (2023) 3752–3765

Contents lists available at ScienceDirect

Petroleum Science

journal homepage: www.keaipublishing.com/en/journals/petroleum-science

Original Paper

Combining unscented Kalman filter and wavelet neural network for anti-slug

Chuan Wang [a, b, *], Long Chen [a, b], Lei Li [c], Yong-Hong Yan [c], Juan Sun [c], Chao Yu [d], Xin Deng [d], Chun-Ping Liang [a], Xue-Liang Zhang [a, b], Wei-Ming Peng [a]

[a] School of Mechanical Engineering, Southwest Petroleum University, Chengdu, 610500, Sichuan, China
[b] Energy Equipment Institute, Southwest Petroleum University, Chengdu, 610500, Sichuan, China
[c] CNPC National Engineering Research Center for Oil and Gas Drilling Equipment Co. LTD, Baoji, 721000, Shaanxi, China
[d] Oil Production Service Co., CETS LTD., Tianjin, 300000, China

ARTICLE INFO

Article history:
Received 31 May 2022
Received in revised form
28 April 2023
Accepted 15 May 2023
Available online 3 June 2023

Edited by Jia-Jia Fei

Keywords:
State estimation
Stable control
Method fusion
Wavelet neural network
Unscented Kalman filter

ABSTRACT

The stability of the subsea oil and gas production system is heavily influenced by slug flow. One successful method of managing slug flow is to use top valve control based on subsea pipeline pressure. However, the complexity of production makes it difficult to measure the pressure of subsea pipelines, and measured values are not always accessible in real-time. The research introduces a technique for integrating Unscented Kalman Filter (UKF) and Wavelet Neural Network (WNN) to estimate the state of subsea pipeline pressure using historical data and a state model. The proposed method treats multiphase flow transport as a nonlinear model, with a dynamic WNN serving as the state observer. To achieve real-time state estimation, the WNN is included into the UKF algorithm to create a WNN-based UKF state equation. Integrate WNN and UKF in a novel way to predict system state accurately. The simulated results show that the approach can efficiently predict the inlet pressure and manage the slug flow in real-time using the riser's top pressure, outlet flow and valve opening. This method of estimate can significantly increase the control effect.

1. Introduction

In deepwater oil and gas development, the mixed fluids produced from wells are typically transported to production platforms for processing. Safe and cost-effective transportation of oil and gas through subsea pipelines is a considerable challenge (Lin et al., 2013). Slug flow is usually a severe problem during transportation (Mao et al., 2016). It is plugs of liquid or gas that travel through the pipeline and can be formed due to transient effects related to pigging, start-up, blow-down, and changes in pressure or flow rates. They are unwanted because they can produce significant pressure fluctuations. When the pressure amplitude is too large, this phenomenon is called severe slug flow and can negatively affect the operation of production facilities.

Researchers have proposed slug catcher, topside choking, full separation, and other techniques to manage extreme slug flow (Ehinmowo and Cao, 2016). Due to the unique characteristics of offshore oil and gas development, today's most common solutions are feedback slug control systems based on the top valve (Storkaas and Skogestad, 2004). To perform anti-slug control in the laboratory, the pipeline inlet pressure is usually measured precisely, and the top valve is employed as a manipulated variable (Godhavn et al., 2005; Sivertsen et al., 2009; Storkaas and Skogestad, 2007). Because of the deep-sea environment, the pipeline inlet pressure cannot be measured directly in the field. As a result, academics employ theoretical methods to determine the slug flow. Backi et al. (2018) proposed a method for estimating the pipeline condition using top pressure and outlet flow to control the slug flow. Aamo et al. (2005) and Di Meglio (2012) developed a state observer for anti-slug control and verified its viability experimentally on this foundation. The observation method's stability, however, is insufficient due to the right half-plane zero point's constraint. For this reason, a virtual flow measurement method to estimate the system's state is proposed by Jahanshahi et al. (2017).

* Corresponding author. School of Mechanical Engineering, Southwest Petroleum University, Chengdu, 610500, Sichuan, China
E-mail address: chuanwang@swpu.edu.cn (C. Wang).

https://doi.org/10.1016/j.petsci.2023.05.008

In 2001, Havre et al. (2001) reported the first industrial application of slug control. They proposed a new control system and implemented it on the Hod-Valhall pipeline. The results showed that when the control system was switched off and the valve opening was kept constant, the slug flow occurred again in the system. This proved that the control system was indeed stabilizing an unstable operating point. In 2003, Skofteland and Godhavn (2003) used a PID controller to stabilize the system flow. The main feature of this approach was the introduction of a cascade control system in which a flow in-loop control system and a pressure out-loop control system were used to jointly suppress severe slug flow. In 2005, Godhavn et al. (2005) reported an application case at the Tordis site. A slug controller was combined with a model to predict and handle liquid slugs entering the separator.

The pipeline and the slug flow inside it can be thought of as a nonlinear dynamic system. The state estimation is now often done using real-time filtering methods such as extended Kalman filter (EKF), UKF, and particle filter (PF) (Kaczmarek, 2016). Among them, the application of EKF to nonlinear system state estimation has been recognized by academia and engineering. But this application has apparent defects (Syre, 2012). The EKF has the characteristic that the overall character of the function is replaced by the local character, and the existence of noise makes it worse. Julier and Uhlmann (1997) offered the UKF approach based on unscented transform to increase the filtering effect of nonlinear issues. In terms of nonlinear filtering, facts show that UKF outperforms EKF (Julier, 2004). In comparison to PF, the calculation cost of UKF is smaller, and the sample weight does not degrade (Arulampalam et al., 2002).

In recent years, artificial intelligence has developed rapidly and neural networks have been widely used in many fields (Lei et al., 2020; Zhao et al., 2019), and WNN is one of them. It is a neural network constructed based on wavelet transform theory, which takes full advantage of the localization of wavelet transform and the large-scale data-parallel processing and self-learning capabilities of neural networks. WNN was initially used for function approximation and speech recognition, and then gradually extended to prediction, classification, and image compression (Guo et al., 2022). Abiyev et al. (2013) combined type-2 fuzzy systems and WNN to propose a novel structure for the identification and control of nonlinear uncertain systems. Xin et al. (2018) proposed a fault detection observer for nonlinear systems based on WNN. Duan et al. (2016) used the WNN algorithm to improve the pattern recognition of surface electromyogram signals. Rajankar and Talbar (2015) used WNN to approximate the signal to maximum accuracy to achieve the denoising of electrocardiographic signals. WNN can accurately identify signals with local singularities, and has strong approximation capability, fast convergence and fault tolerance. It has been practiced successfully in the field of prediction and control (Xia et al., 2020).

In this article, WNN is used to create a high-precision state model that thoroughly learns the dynamic properties of the pipeline's slug flow. To estimate and control the real-time slug flow with high accuracy, a new method of subsea pipeline pressure estimation is established by combining dynamic WNN and improving UKF. The rest of this paper is as follows: Section 2 describes previous state estimation and control methods for severe slug flow; Section 3 and section 3.2 elaborate the proposed real-time state estimation method that combines WNN and UKF; Section 4 shows the validation of the proposed method and the comparison with traditional methods; Section 5 draws conclusions and ends the full text.

2. Background

Since the 1970s, Xiao et al. (1990), Taitel and Dukler (1977), and others have developed slug flow dynamics models. These models are mainly used to describe the flow parameters of slug flow, such as liquid slug length, liquid slug velocity, liquid slug frequency, etc. The goal of these models is to investigate the slugging process and slug flow stability. Following that, various transient models describing slug flow appeared, and a few commercial software, such as OLGA, was created based on these models (Bendlksen et al., 1991). The nonlinear partial differential equations (PDE) of two-phase or three-phase flow, which include continuous equations, momentum conservation equations, energy conservation equations and associated closure equations, are the foundations for these transient models. It can simulate severe slug flow generated in laboratory and oilfield systems with reasonable accuracy, but it is not suitable for real-time slug control due to the complicated parameters. After this, scholars such as Storkaas et al. (2003) and Meglio (2009) have simplified the accuracy and complexity of the PDE slug flow model and developed models based on the ordinary differential equation (ODE).

Jahanshahi and Skogestad (2011) proposed an ODE model based on the conservation of mass at each stage of the pipeline and riser. The model includes a section of subsea horizontal pipeline, subsea downward-dipping pipeline, riser section, and platform horizontal pipeline. In the process of model establishment, it is assumed that the gas in the pipeline conforms to the ideal gas equation, and the liquid is incompressible. It has been proved that this model has similar dynamic characteristics to the OLGA simulator and can describe the state of slug flow. Fig. 1 is a description of this model.

Please refer to Appendix A for more information about the ODE model, which has a detailed description of the pipeline-riser system and model derivation. The ODE model has the advantages of fewer parameters and excellent dynamic response. Syre (2012) combined the model with EKF and UKF, respectively, to form an observer. The simulation results showed that EKF worked well locally. UKF worked best with high input disturbances and was more robust. The observers were combined with proportional integral (PI) controller, linear quadratic regulator (LQR), and model predictive control (MPC), respectively, for slug flow control. However, this control scheme was unstable under input perturbations and increasing valve openings.

Jahanshahi et al. (2013b) applied this model to propose an anti-slug controller whose convergence was proved in theory and experiments. The controller directly used the pressures at the riser-base and the riser top. The controllability limitation of utilizing

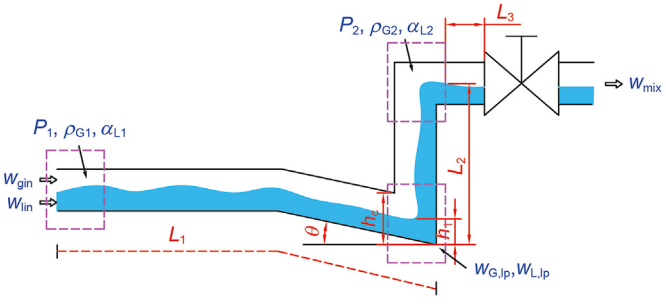

Fig. 1. Pipeline-riser simplified model with critical parameters.

riser-base pressure was the small gain of the systems with large valve openings. No control method could address a limitation in nonlinearity and non-minimum phase dynamics with riser top pressure.

Oliveira et al. (2015) used the ODE model to propose a control method that could quickly identify and adapt to system changes. The scheme consisted of an autonomous detector and adaptive controller that manipulated the pressure set point to maximize throughput. Jahanshahi and Skogestad (2017) conducted nonlinear and linear analyses and evaluated four control designs experimentally with both subsea and topside pressures. It was demonstrated that the system could be stabilized by using a nonlinear high-gain observer and controlling estimation in the case of unmeasurable pipeline inlet pressure. But this solution was only suitable for small valve openings.

Based on the ODE model, Jahanshahi et al. (2013a) compared the control effects of several different observers, among which the UKF sometimes did not stabilize the system. This may be since the ODE models assume that the state within the pipeline varies linearly. The simple linearity assumption limits the accuracy of the estimation. When the model is used for nonlinear processes, considerable deviations in accuracy and efficiency occur, and the accuracy of UKF prediction is affected. Therefore, WNN with strong nonlinear mapping capability is chosen to be introduced into UKF. Since the wavelet function is an orthogonal local approximation function and can translate and scale in space. It has good time-frequency resolution performance when the system changes sharply, and the neural network can improve the resolution scale to ensure the accuracy of approximation (Guo et al., 2022). In addition, due to the orthogonality of the function bases, adding or removing network nodes during the training process does not affect the trained network weights, which can greatly reduce the network learning time. The compact combination of wavelet transform and neural network fully integrates the advantages of both (Ramadevi and Bingi, 2022). Compared with traditional neural networks, WNN has stronger memory ability for nonlinear functions and has great improvement in convergence speed, approximation accuracy, and generalization performance. The system established by WNN identification can approximate the dynamic properties of the system well on the model (Forootan et al., 2022). The fusion of UKF and WNN can better cope with the relatively large fluctuation of inlet flow and top valve flow and enhance the robustness of the system to handle the slug flow with a new state estimation method.

3. UKF based on WNN for state estimation

This section aims to explain the UKF fused with WNN for state estimation. The core idea is as follows. Considering the subsea multiphase flow transport as a nonlinear model, the WNN can form a transfer function for the improved UKF and constitute the best state equation of the UKF. In real-time observations, the gas-liquid quality changes of the subsea pipeline-riser are inevitably mixed with the process noise. Due to the framework of the UKF, the one-step prediction of the subsea pipeline pressure can be corrected immediately by updating during the measurement update stage. In this section, the UKF algorithm based on WNN is explained in detail, and a fusion method is designed to ensure the effectiveness of the combination of UKF and WNN, which is the focus of this article.

3.1. State and measurement equations for fusion WNN

During the derivation of the ODE model, there is some mapping relationship between the pipeline inlet pressure P_1 and the riser top pressure P_2, the outlet flow w_{out}, and the valve opening u. Therefore, $P_{1(k-1)}$, $P_{2(k)}$, $w_{\text{out}(k)}$, $u_{(k)}$ are used as input and $P_{1(k)}$ as output to train the WNN. In this paper, a wavelet neural network with continuous parameters is used, and its structure is shown in Fig. 2. The number of neurons in the input layer is N, and the number of neurons in the hidden layer is J.

1. Input layer: Normalize the $P_{1(k-1)}$, $P_{2(k)}$, $w_{\text{out}(k)}$, $u_{(k)}$ collected by the sensor as the training input.
2. Hidden layer: The Morlet wavelet function will be used as the mother wavelet function in this paper. The Morlet wavelet function is continuous and derivable, having good time-frequency local characteristics. It is relatively simple to express. The mathematical formula is:

$$\Psi(x) = C\cos(5x)\mathrm{e}^{-x^2/2} \tag{1}$$

In the formula, C is the normalization constant during reconstruction.

Increase the translation factor and expansion factor. The output of each node can be expressed as:

$$h(j) = \Psi\left(\frac{\sum_{n=1}^{N}\omega_{jn}x_n - \beta_j}{\alpha_j}\right), n = 1,2,\cdots,N \quad j = 1,2,\cdots,J \tag{2}$$

Among them, h_j is the output of the jth neuron in the hidden layer obtained through the action of the wavelet framework. β_j is the translation factor. α_j is the expansion factor and ω_{jn} is the connection weight of the jth neuron in the hidden layer to the nth neuron in the input layer.

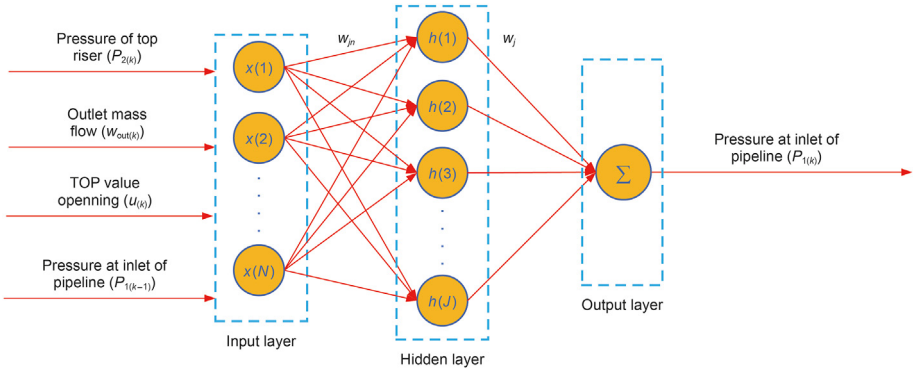

Fig. 2. WNN structure.

3. Output layer: The output layer is a linear combination of the wavelet framework, which can be expressed as:

$$y_{(k)} = \sum_{j=1}^{J} \omega_j h(j), j = 1, 2, \cdots, J \tag{3}$$

where, ω_j is the connection weight of the jth neuron in the hidden layer to the output layer.

4. Parameter update: The wavelet network uses a weight correction algorithm, using the gradient to correct the weights of the wavelet network and the parameters of the wavelet function, so that the wavelet network continuously approximates the expected output. Here, the mean square error (MSE) is used as the error function. The iterative process can be expressed as follows:

Calculation error:

$$\mathrm{MSE} = \frac{1}{M}\sum_{k=1}^{M}(y_k - \hat{y}_k)^2 \tag{4}$$

Correction parameters:

$$\begin{aligned} \omega_{n,k}^{(i+1)} &= \omega_{n,k}^{i} + \Delta\omega_{n,k}^{(i+1)} \\ a_k^{(i+1)} &= a_k^{i} + \Delta a_k^{(i+1)} \\ b_k^{(i+1)} &= b_k^{i} + \Delta b_k^{(i+1)} \end{aligned} \tag{5}$$

Among them, $\Delta\omega_{n,k}^{(i+1)}, \Delta a_k^{(i+1)}, \Delta b_k^{(i+1)}$ can be calculated according to the error:

$$\begin{aligned} \Delta\omega_{n,k}^{(i+1)} &= -\eta\frac{\partial e}{\partial \omega_{n,k}^{(i)}} \\ \Delta a_k^{(i+1)} &= -\eta\frac{\partial e}{\partial \alpha_k^{(i)}} \\ \Delta b_k^{(i+1)} &= -\eta\frac{\partial e}{\partial b_k^{(i)}} \end{aligned} \tag{6}$$

where, η is the learning rate. Combining with Eqs. (1)–(3), the mapping relationship inside WNN can be expressed more clearly by weight matrix as follows:

$$\hat{P}_{1(k)} = y_{(k)} = \mathbf{U}\cdot\Psi\left(\frac{\mathbf{S}\cdot x_{\mathrm{input},n} - b}{a}\right) = f(x_{\mathrm{input},n}), n = 1, 2, \cdots, N \tag{7}$$

In the formula, $x_{\mathrm{input},n} = \begin{bmatrix} P_{2(k)} & w_{\mathrm{out}(k)} & u & P_{1(k-1)} \end{bmatrix}^T$ represents the input of WNN, and $b = \begin{bmatrix} b_1 & b_2 & \cdots & b_J \end{bmatrix}^T$ represents the translation factor vector, and $a = \begin{bmatrix} a_1 & a_2 & \cdots & a_J \end{bmatrix}^T$ represents the expansion factor vector, and $\mathbf{S}$ is the weight matrix from the input layer to the hidden layer, and $\mathbf{U}$ is the weight matrix from the hidden layer to the output layer, which are defined as:

$$\mathbf{S} = \begin{bmatrix} \omega_{11} & \omega_{12} & \cdots & \omega_{1N} \\ \omega_{21} & \omega_{22} & \cdots & \omega_{2N} \\ \vdots & \vdots & \ddots & \vdots \\ \omega_{J1} & \omega_{J2} & \cdots & \omega_{JN} \end{bmatrix} \tag{8}$$

$$\mathbf{U} = \begin{bmatrix} \omega_1 & \omega_2 & \cdots & \omega_J \end{bmatrix} \tag{9}$$

In the continuous prediction process of P_1, $f(\cdot)$ represents the internal state of WNN. It is continuously changed and updated over time during state estimation. The WNN is integrated into the UKF framework. Its state and measurement equations are as follows:

$$x_k = \begin{bmatrix} P_2 \\ \omega_{\mathrm{out}} \\ u \\ P_1 \end{bmatrix}_k + w_{k-1} = \begin{bmatrix} \begin{bmatrix} 1 & 0 & 0 \\ 0 & 1 & 0 \\ 0 & 0 & 1 \end{bmatrix} & \begin{bmatrix} P_2 \\ \omega_{\mathrm{out}} \\ u \end{bmatrix} \\ f([\,P_2 \quad \omega_{\mathrm{out}} \quad u \quad P_1\,]) \end{bmatrix}_{k-1} + w_{k-1} \tag{10}$$

$$z_k = H(x_k) + v_k \tag{11}$$

where x_k is the system state and $f(\cdot)$ is the nonlinear transfer function at time k in the WNN. w_{k-1} is random process noise and has a covariance matrix $\mathbf{Q}_{k-1}$. v_k is random measurement noise and has a covariance matrix $\mathbf{R}_k$. $z_k = [\,P_2 \quad \omega_{\mathrm{out}} \quad u\,]^T$ is the observation vector and $H = \begin{bmatrix} 1 & 0 & 0 & 0 \\ 0 & 1 & 0 & 0 \\ 0 & 0 & 1 & 0 \end{bmatrix}$ is the measurement function. The initial state x_0 is independent of all noise, and its prior mean and covariance matrix are:

$$E(x_0) = \bar{x}_0 = \hat{x}_{0|0},\ \mathrm{cov}(x_0) = P_0 \tag{12}$$

3.2. Algorithm of UKF based on WNN

3.2.1. Initialization

The state estimate $\hat{x}_{k-1|k-1}$ and the error covariance matrix $P_{k-1|k-1}$ are initialized according to the initial gas and liquid flow. Initialize the output of the WNN hidden layer as $h_j = O_J$, where O_J is an all-zero column vector of length J.

3.2.2. Sampling at σ points

(1) Calculate σ point weight coefficient:

$$\begin{cases} \omega_0^{(\mathrm{m})} = \lambda\big/(n+\lambda) \\ \omega_0^{(\mathrm{c})} = \lambda\big/(n+\lambda) + \left(1 - \alpha^2 + \beta\right) \\ \omega_i^{(\mathrm{m})} = \omega_i^{(\mathrm{c})} = \dfrac{0.5}{(n+\lambda)},\ i = 1, 2, \cdots, 2n \end{cases} \tag{13}$$

Among them, n is the state space dimension, and $\lambda = \alpha^2(n+\kappa) - n$ is a comprehensive factor. α determines the dispersion degree of σ points, usually being a small positive value (such as 0.01), and κ is usually $3 - n$. β is used to describe the distribution information of x. In the case of Gauss distribution, the optimal value of β is 2. $\omega_i^{(\mathrm{m})}$ is the weight coefficient when seeking first-order statistical characteristics, and $\omega_i^{(\mathrm{c})}$ is the weight coefficient when seeking second-order statistical characteristics.

(2) Calculate the σ point $\xi_{k-1|k-1}^{(i)}(i = 0, 1, \cdots, 2n)$:

$$\begin{cases} \xi_{k-1|k-1}^{(0)} = \hat{x}_{k-1|k-1} \\ \xi_{k-1|k-1}^{(i)} = \hat{x}_{k-1|k-1} + \left(\sqrt{(n+\lambda)P_{k-1|k-1}}\right)_i, i = 1, 2, \cdots, n \\ \xi_{k-1|k-1}^{(i)} = \hat{x}_{k-1|k-1} - \left(\sqrt{(n+\lambda)P_{k-1|k-1}}\right)_i, i = n+1, n+2, \cdots, 2n \end{cases} \tag{14}$$

In the formula, $\hat{x}_{k-1|k-1}$, $P_{k-1|k-1}$ represents the initial state and error covariance matrix, and $(\sqrt{(n+\lambda)P_{k-1|k-1}})_i$ represents the ith column of the square root of the matrix.

3.2.3. Time update

When WNN and UKF are directly combined, there is a contradiction. According to the structure of WNN, WNN is dynamic. Because of continuous input, its internal state is constantly updated, and the nonlinear transfer function formed by WNN is also dynamic. In the time update phase, the input of the nonlinear transfer function is only the σ point, so for any two consecutive σ points, the corresponding nonlinear transfer function will not be the same. However, according to the standard UKF algorithm, each σ point should be transformed according to the same nonlinear transfer function in unscented transformation. In other words, once the unscented transformation is applied, the transfer function in the state equation should be completely static. Therefore, there is a contradiction between the update of the nonlinear transfer function and the effective conversion of the σ point. The method which solves this problem is shown in Fig. 3.

(1) σ point transformation

The Eq. (10) can be simplified as:

$$x_k = F(x_{k-1}) + w_{k-1} \tag{15}$$

where $F(\cdot)$ is the transfer function at time k. Transform the σ points from 1 to $2n$ through the non-linear input-output transfer function of WNN:

$$\xi_k^{(i)} = F\left(\xi_{k-1|k-1}^{(i)}\right),\ i = 1, 2, \cdots, 2n \tag{16}$$

In the formula, $\xi_{k|k}^{(i)}$ represents the next prediction of σ points. In the standard UKF algorithm, the transfer function $F(\cdot)$ is determined by the state model, but the WNN is introduced into the UKF framework. To obtain the transfer function at this time, the dynamic WNN is regarded as a static nonlinear function briefly, where the value of $f(\xi_{k-1|k-1}^{(i)})$ is calculated separately by input $x_{\text{input},i} = \xi_{k-1|k-1}^{(i)} (i = 1, 2, \cdots, 2n)$. This transformation can be seen as independently applying the same state to each σ point. It is worth noting that after the entire process, the internal state of the WNN has not been updated at this time. $\xi_{k-1|k-1}^{(i)} (i = 1, 2, \cdots, 2n)$ is not a continuous input of a dynamic WNN, but an independent input to the transfer function at this time. Therefore, at time K, the prediction of each σ point can be calculated separately.

(2) WNN status update

Convert the σ point through the transfer function:

$$\xi_k^{(0)} = F\left(\xi_{k-1|k-1}^{(0)}\right) \tag{17}$$

At time K, $\xi_{k-1|k-1}^{(0)}$ is regarded as the input of the dynamic WNN, i.e. $x_{\text{input},k} = \xi_{k-1|k-1}^{(0)}$, to get $f(\xi_{k-1|k-1}^{(0)})$. At this moment, the prediction of $\xi_{k-1|k-1}^{(0)}$ is also calculated based on the same WNN internal state in the previous step. But after this process, the internal state of WNN has been updated. After $\xi_k^{(0)}$ is obtained, the input-output function of WNN has changed, which provides a basis for the time update in the next stage.

Through the methods in Eqs. (1) and (2), the nonlinear transfer function in UKF becomes dynamic during the entire observation process, because WNN is updated after each time step. Therefore, it can keep track of the trend of state changes. In a certain time step, the transfer function is static, which ensures that each σ point is converted based on the same transfer function at the same time.

(3) State estimation and measurement value prediction:

$$\begin{cases} \hat{x}_{k|k-1} = \sum_{i=0}^{2n} \omega_i^{(m)} \xi_k^{(i)} \\ P_{k|k-1} = \sum_{i=0}^{2n} \omega_i^{(c)} \left(\xi_k^{(i)} - \hat{x}_{k|k-1}\right)\left(\xi_k^{(i)} - \hat{x}_{k|k-1}\right)^{\mathrm{T}} + Q_{k-1} \end{cases} \tag{18}$$

where $\hat{x}_{k|k-1}$ denotes the estimated state and $P_{k|k-1}$ denotes the covariance matrix of the error.

When calculating the predicted measurement value $\hat{z}_{k|k-1}$ and its error covariance matrix $P_{\tilde{z}_k}$, generating σ points can be skipped. The generated predicted points are directly brought into the measurement equation. The process is as follows:

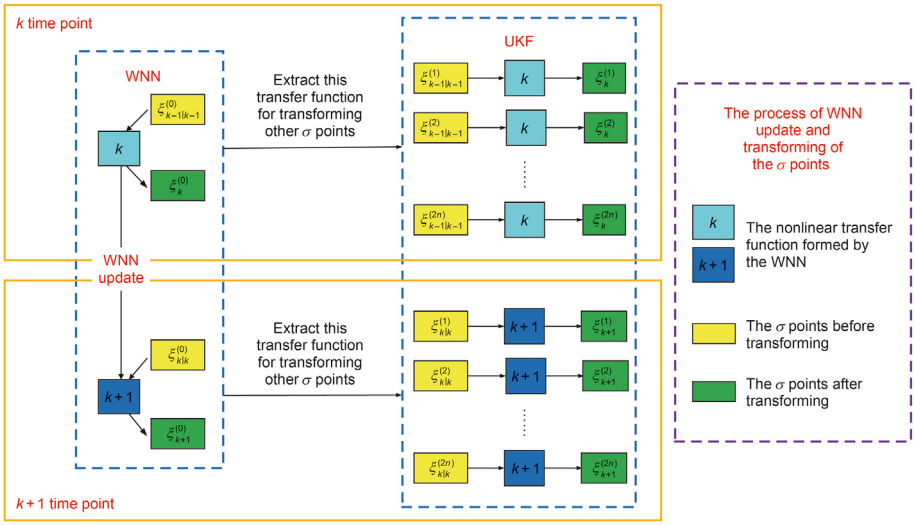

Fig. 3. Contradictory solution.

$$\begin{cases} \psi_k^{(i)} = H\left(\xi_k^{(i)}\right), i = 0, 1, \cdots, 2n \\ \widehat{z}_{k|k-1} = \sum_{i=0}^{2n} \omega_i^{(\mathrm{m})} \psi_k^{(i)} \\ P_{\tilde{z}_k} = \sum_{i=0}^{2n} \omega_i^{(\mathrm{c})} \left(\psi_k^{(i)} - \widehat{z}_{k|k-1}\right)\left(\psi_k^{(i)} - \widehat{z}_{k|k-1}\right)^{\mathrm{T}} + R_k \\ P_{\tilde{x}_k \tilde{z}_k} = \sum_{i=0}^{2n} \omega_i^{(\mathrm{c})} \left(\xi_k^{(i)} - \widehat{x}_{k|k-1}\right)\left(\psi_k^{(i)} - \widehat{z}_{k|k-1}\right)^{\mathrm{T}} \end{cases} \tag{19}$$

In the formula, $\psi_{k|k}^{(i)}$ represents the predicted measurement corresponding to the σ point, and $\widehat{z}_{k|k-1}$ represents its mean, and $P_{\tilde{z}_k}$ represents its error covariance matrix. $P_{\tilde{x}_k \tilde{z}_k}$ represents the cross covariance matrix of the state estimation and the predicted measurement.

3.2.4. Measurement update

After obtaining the measurement z_k, the best state estimate $\widehat{x}_{k|k}$, the gain matrix K_k, and the updated error covariance matrix $P_{k|k}$ can be obtained:

$$\begin{cases} \widehat{x}_{k|k} = \widehat{x}_{k|k-1} + K_k\left(z_k - \widehat{z}_{k|k-1}\right) \\ K_k = P_{\tilde{x}_k \tilde{z}_k} P_{\tilde{z}_k}^{-1} \\ P_{k|k} = P_{k|k-1} - K_k P_{\tilde{z}_k}^{-1} K_k^{\mathrm{T}} \end{cases} \tag{20}$$

According to historical data, WNN learns through training samples, and each sample consists of an input vector and a target. Therefore, the trained WNN can learn the dynamic characteristics of the multiphase flow in the mixed transmission pipeline. It can accurately predict the pipeline inlet pressure and continuously update its internal state. However, the nonlinear transfer function in the UKF framework is not updated over time, so $\xi_{k-1|k-1}^{(0)}$ is selected as the input of WNN at time K. It is transformed by the nonlinear transfer function and updates the WNN, but other σ points cannot be continuous input of the WNN, otherwise the internal state of the WNN will be updated. As a result, in the real-time estimation of fusing WNN and UKF, WNN provides an essential basis for time update in UKF. At the same time, the framework of UKF can provide accurate input for WNN in real-time and promote WNN updates. The whole algorithm framework is shown in Fig. 4.

4. Results and discussion

The experiments of real-time estimation and slug flow control using the WNN-UKF algorithm are introduced in this section to prove the applicability and superiority of the method.

4.1. Experimental setup

Fig. 5 is the schematic diagram of the experimental setup. The pipeline and riser are made of flexible pipes with an inner diameter of 15 cm. The length of the pipe is 5000 m, and the inclination angle is 15°. The height of the riser is 30 m, and the top is installed with a top valve. The Xmas tree on the far left is connected to the multiphase pipeline. A multiphase flowmeter is used at the inlet to measure the flow rates of the gas and liquid phases. The collected data is pipeline inlet pressure P_1, top valve opening u, riser top pressure P_2, and outlet flow w_{out}.

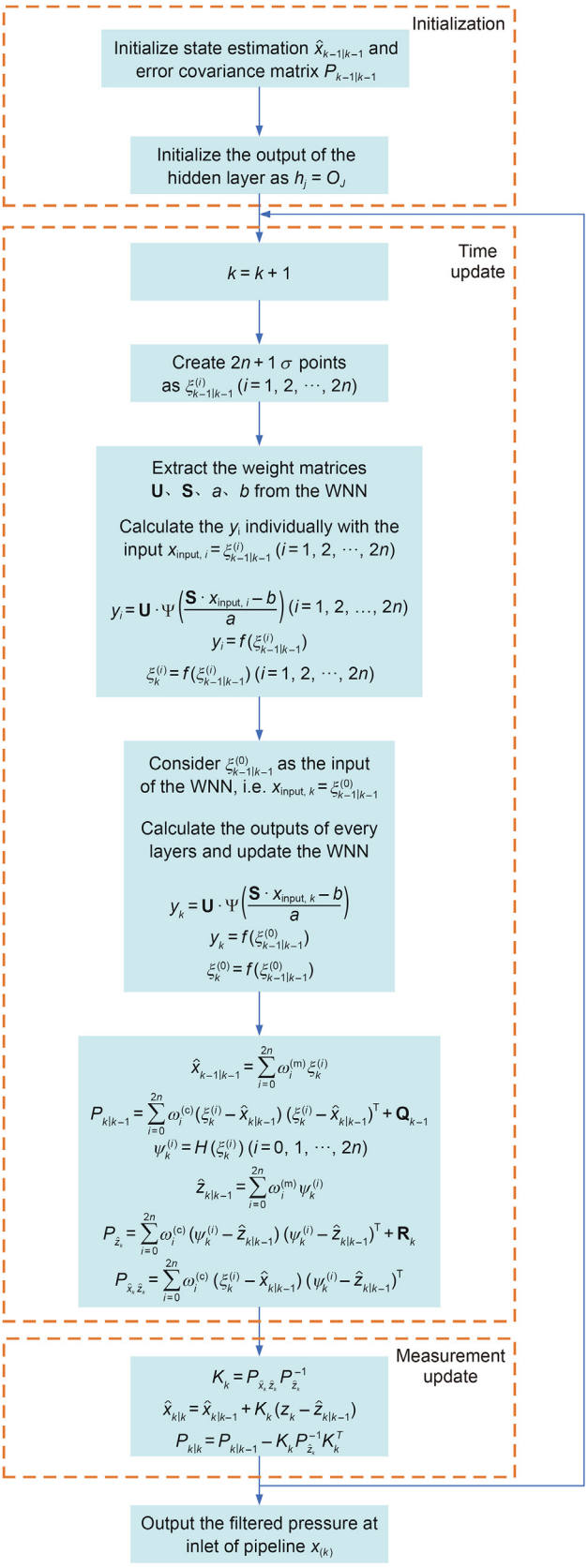

Fig. 4. WNN-UKF algorithm.

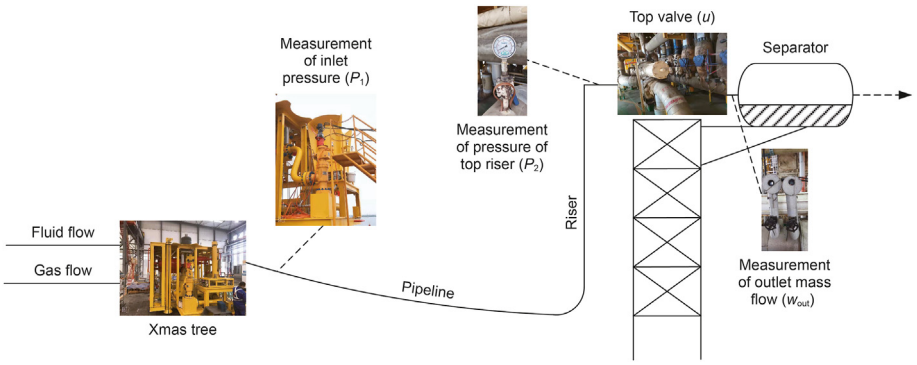

Fig. 5. Schematic diagram of the experimental device.

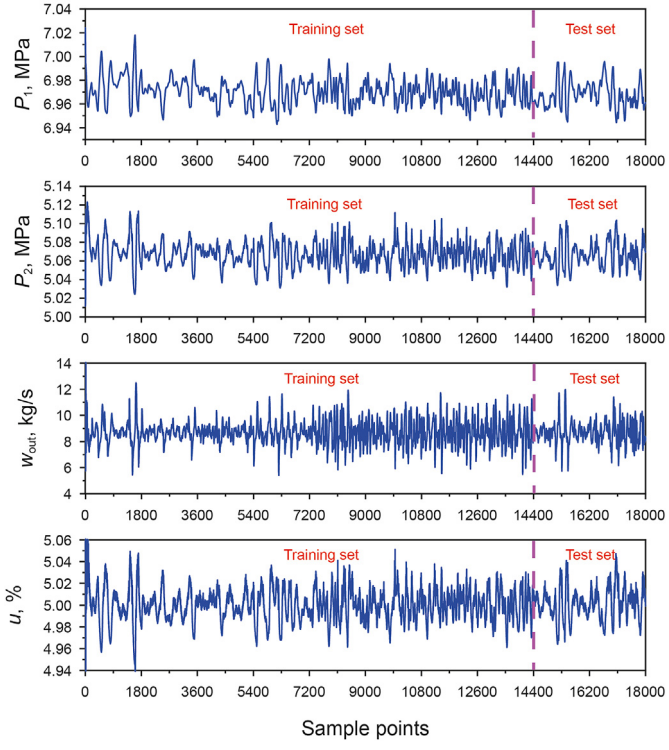

Fig. 6. Training and testing data sets.

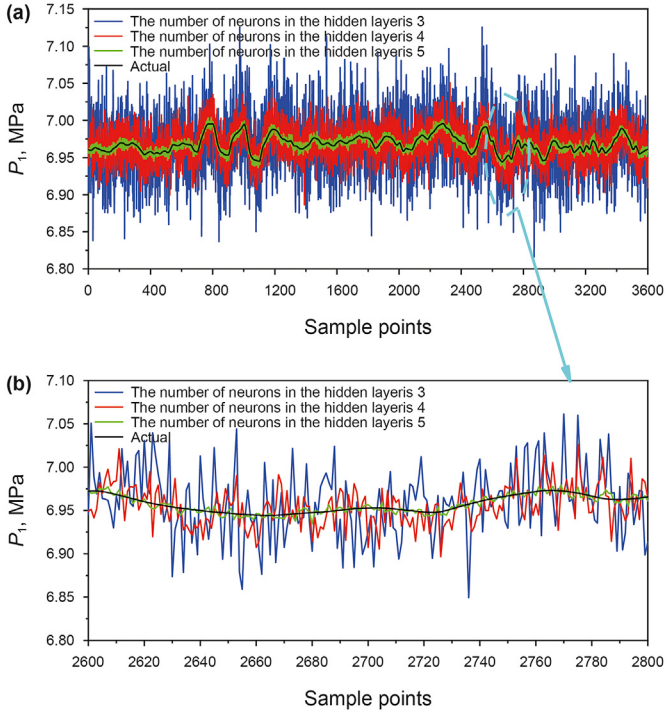

Fig. 7. (**a**) Comparison results of the different number of neurons in the hidden layer. (**b**) The enlarged part of (**a**).

4.2. Analysis of results

The above device continuously collects eighteen thousand data points. The first 14,400 data points are used to train WNN. The dataset is shown in Fig. 6. To study the fitting characteristics of WNN and set the appropriate number of nodes in the hidden layer, the number of different neurons in the hidden layer is compared. The number is set to 3, 4, 5, 6, 7, and 8 respectively. The number of neurons in the input layer is $N = 4$. After the WNN training is completed, the last 3600 data points are used for testing and comparison, and the results are shown in Figs. 7 and 8.

The data collected by the above device for 5 h are the subsea pipeline pressure P_1, the top valve opening u, the top pressure P_2, and the flow rate w_{out}. Take the first 4 h of data for training and the last hour of data for verification. The data set is shown in Fig. 6. Mean square error (MSE) is used as an evaluation parameter, which is defined as Eq. (21), and the results are shown in Table 1.

$$\mathrm{MSE} = \frac{\sum_{i=1}^{m} (y_i - \hat{y}_i)^2}{m} \tag{21}$$

In the formula, y_i represents the actual value, and $\hat{y}_i$ represents the estimated value, and m represents the number of samples.

The above results reflect that when the number of neurons increases from 3 to 5, the MSE decreases from 1.591e-3 to 1.323e-5. But when the number of neurons continues to increase, the MSE gradually increases. It may be that the limited amount of information contained in the training set is not sufficient to train all the neurons, thus leading to overfitting. Even if the training data contains enough information, excessive neurons will increase the training time, making it difficult to achieve the expected prediction accuracy. For this reason, the number of hidden layer neurons is chosen to be 5 for constructing the estimation model.

To compare the one-step state estimation of different models built by WNN and ODE, the same test set was used to examine their

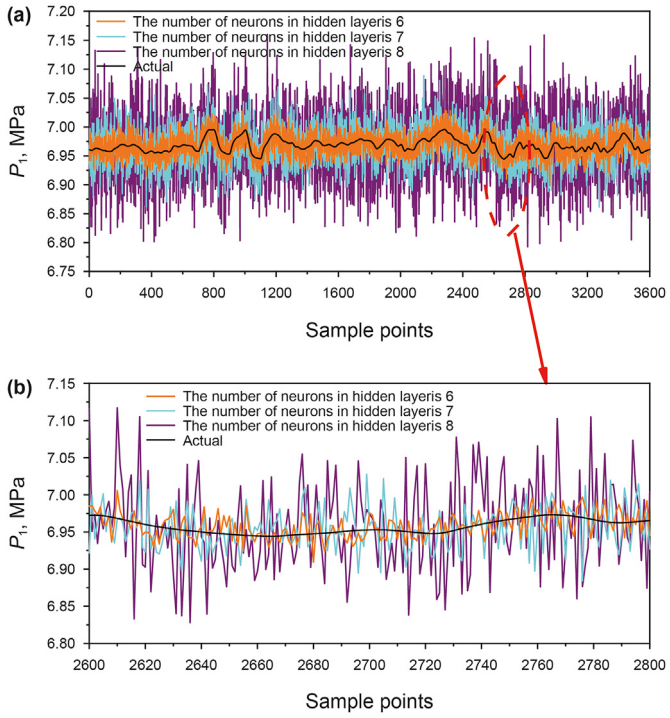

Fig. 8. (**a**) Comparison results of the different number of neurons in the hidden layer. (**b**) The enlarged part of (**a**).

Table 1
Accuracy analysis of the different number of neurons in hidden layers.

Number of neurons in hidden layers	MSE, MPa
3	1.591e-3
4	4.055e-4
5	1.323e-5
6	2.413e-4
7	8.743e-4
8	3.100e-3

prediction accuracy. The initial parameters of the system are shown in Table 2, and Fig. 9 shows the comparison results. Fig. 10 shows the squared estimation error for both models. To quantitatively compare the prediction accuracy of different models, Table 3 lists the statistical analysis of prediction errors, including mean absolute error (MAE) and root mean squared error (RMSE), which are defined as follows:

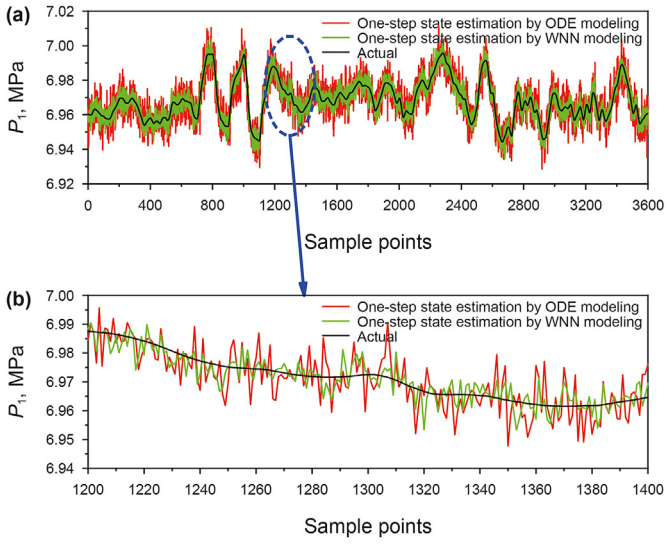

Fig. 9. (**a**) Comparison of one-step state estimation of different models established by WNN and ODE. (**b**) The enlarged part of (**a**).

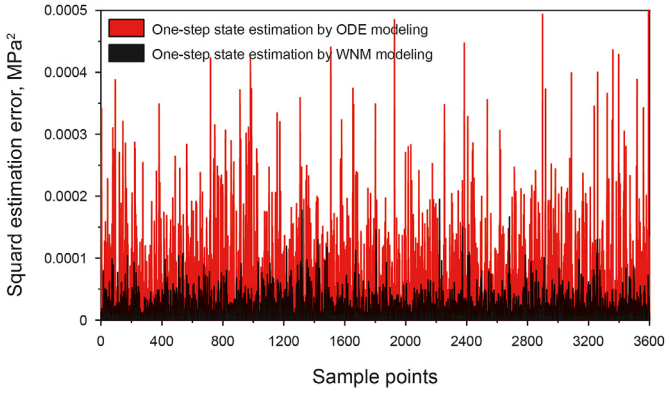

Fig. 10. Comparison of squared estimation errors.

$$\mathrm{MAE} = \frac{\sum_{i=1}^{m} |y_i - \hat{y}_i|}{m} \tag{22}$$

Table 2
Model initial parameters.

Parameter	Value	Description
P_0	5 MPa	Top separator pressure
w_c	0.17	Moisture content
ρ_l	832.2 kg/m^3	Liquid density
M_g	18 gr	Gas molecular mass
μ	1.426×10^{-4} Pa•s	Viscosity
R	8314 J/(mol·K)	Gas constant
C_{top}	3.3×10^{-3}	Top valve coefficient
K_g	3.49×10^{-2}	Gas flow coefficient at the bottom of the riser
K_l	2.81×10^{-1}	Liquid flow coefficient at the bottom of the riser
D_p	0.25 m	Diameter of subsea pipeline
D_r	0.25 m	Diameter of riser
w_{nom}	9 kg/s	Nominal flow
T_1	369 K	Pipe inlet temperature
T_2	298 K	Top temperature of riser

Table 3
Comparison of estimation accuracy of different models.

Model	MAE, MPa	RMAE, MPa
ODE	5.413e-3	6.793e-3
WNN	2.923e-3	3.747e-3

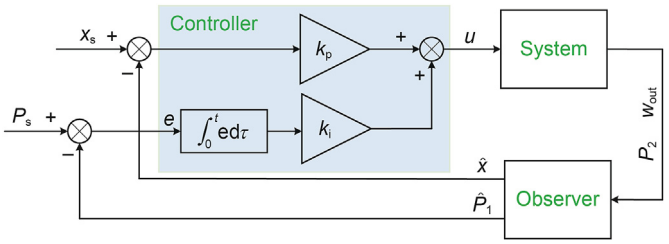

Fig. 11. Feedback control block diagram.

$$\mathrm{RMSE} = \sqrt{\frac{\sum_{i=1}^{m} (y_i - \hat{y}_i)^2}{m}} \tag{23}$$

In the formula, y_i represents the actual value, and $\hat{y}_i$ represents the estimated value, and m represents the number of samples. All the comparison results indicate that in the one-step state estimation, compared with the ODE model, the WNN model has a smaller estimation error and can better reflect the dynamic changes of gas and liquid in the pipeline. It is more suitable for fusion with UKF to form a new observer.

To verify the effectiveness of the observation system, the PI controller is combined for real-time control of the system. As shown in Fig. 11, the full state feedback is applied by using the estimated states. Also, to prevent deviations from the set pipeline inlet pressure P_s, the integral action is added by integrating the deviation values. The overall control action can be expressed as (Jahanshahi and Skogestad, 2017):

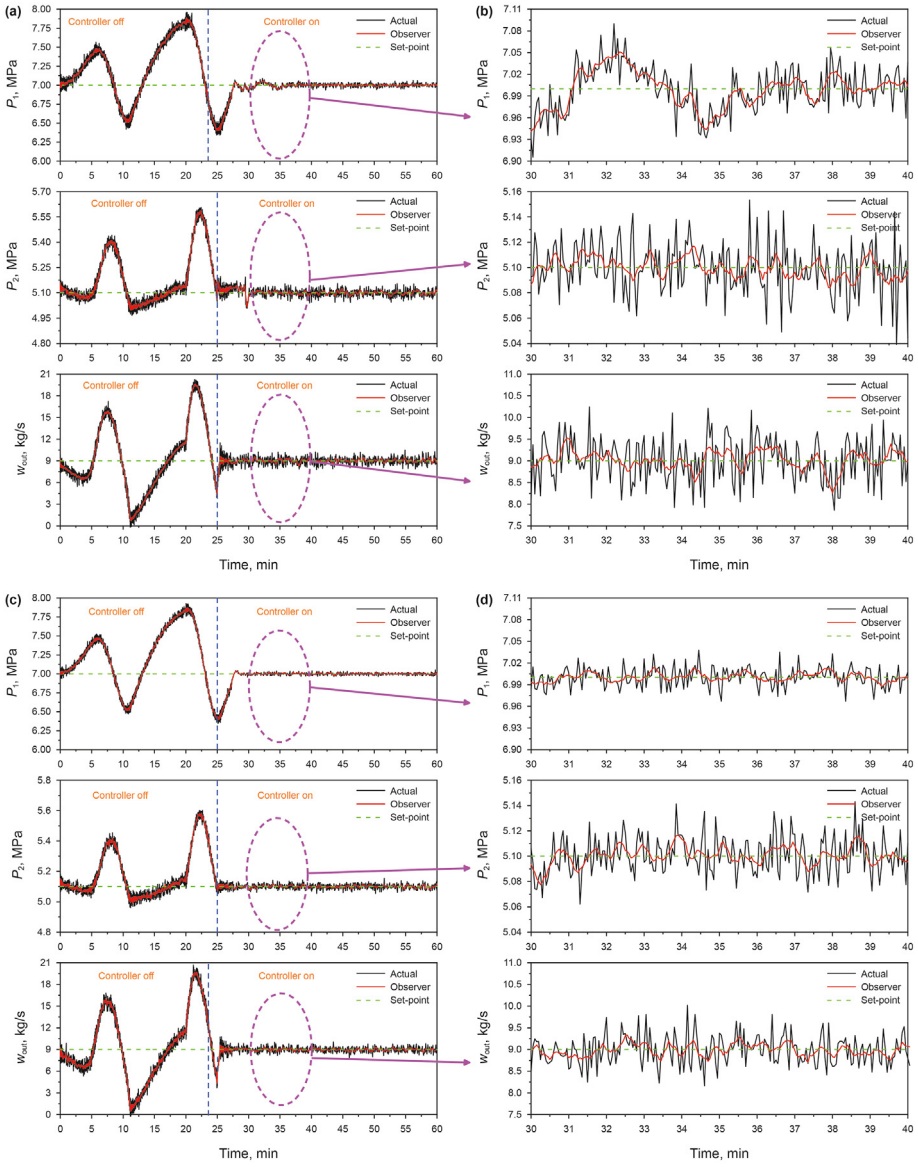

Fig. 12. Real-time control effect using different observers with 10% valve opening. (**a**) ODE-UKF as observer. (**b**) The enlarged part of (**a**). (**c**) WNN-UKF as observer. (**d**) The enlarged part of (**c**).

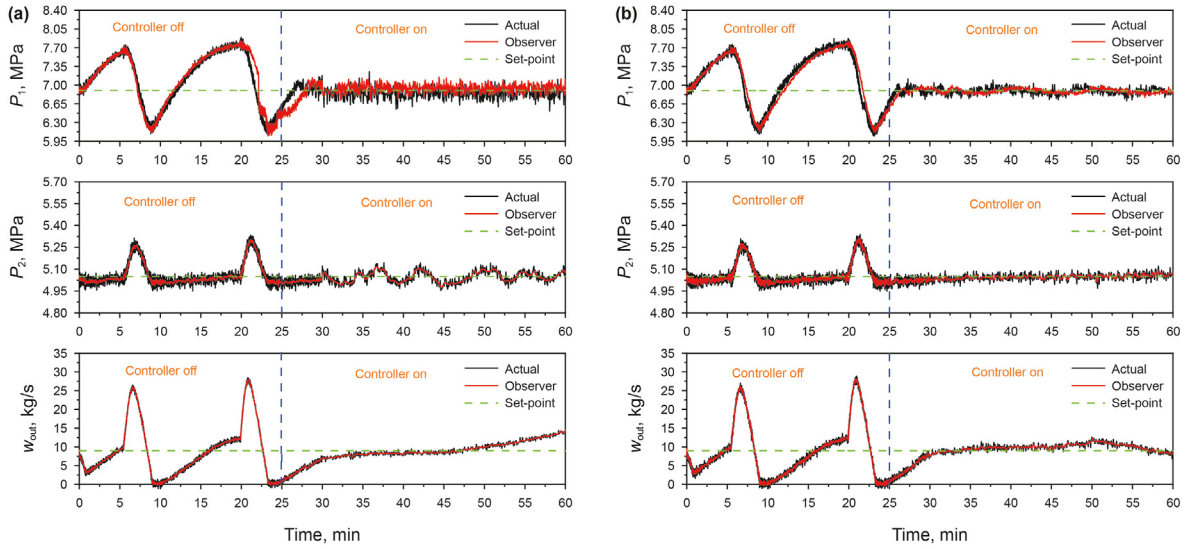

Fig. 13. Real-time control effect using different observers with 15% valve opening. (**a**) ODE-UKF as observer. (**b**) WNN-UKF as observer.

Table 4
Comparison of errors of different control systems.

Valve opening	Observer	ISE	IAE
10%	ODE-UKF	2.85	2.98
	WNN-UKF	0.73	0.85
15%	ODE-UKF	3.65	3.82
	WNN-IKF	1.26	1.41

$$u(t) = -K_p(\hat{x}(t) - x_s) + K_i \int_0^t (\hat{P}_1(\tau) - P_s)\mathrm{d}\tau \tag{24}$$

where K_P is the linear optimal controller calculated by solving the Riccati equation, and K_i is a relatively small integral gain ($K_i = 0.01$). MATLAB is used to simulate the multiphase flow transmission and set the variance of P_2 and w_{out} measurement noise to be 0.33% of the observed mean. The gas flow rate at the inlet is $w_{g.in} = 0.34$ kg/s, and the liquid flow rate is $w_{l.in} = 8.60$ kg/s. To test the robustness of the control system, Gaussian white noise is added to the input flow. Under these boundary conditions, the valve opening where the system switches from stable (non-slug) to oscillatory is at $u = 15\%$ (Jahanshahi and Skogestad, 2011). The steady-state in the slug condition is unstable but can be stabilized by control. u is set to 10%, 15%, and 20%, respectively, to compare the control performance of different observation methods.

The controller is turned on at 25 min and held for 35 min. It can be seen from Fig. 12(a) and (c) that when the valve opening is 10%, both ODE-UKF and WNN-UKF can stabilize the system as observers. However, by comparing (b) and (d), it can be seen that the actual value of WNN-UKF is closer to the set-point. As the valve opening increases, it becomes more difficult for the control system to stabilize (Jahanshahi et al., 2012). When the valve opening increases to 15%, in Fig. 13(a), the system state is near the set value but fluctuates frequently. Obviously, with ODE-UKF as the observer, the

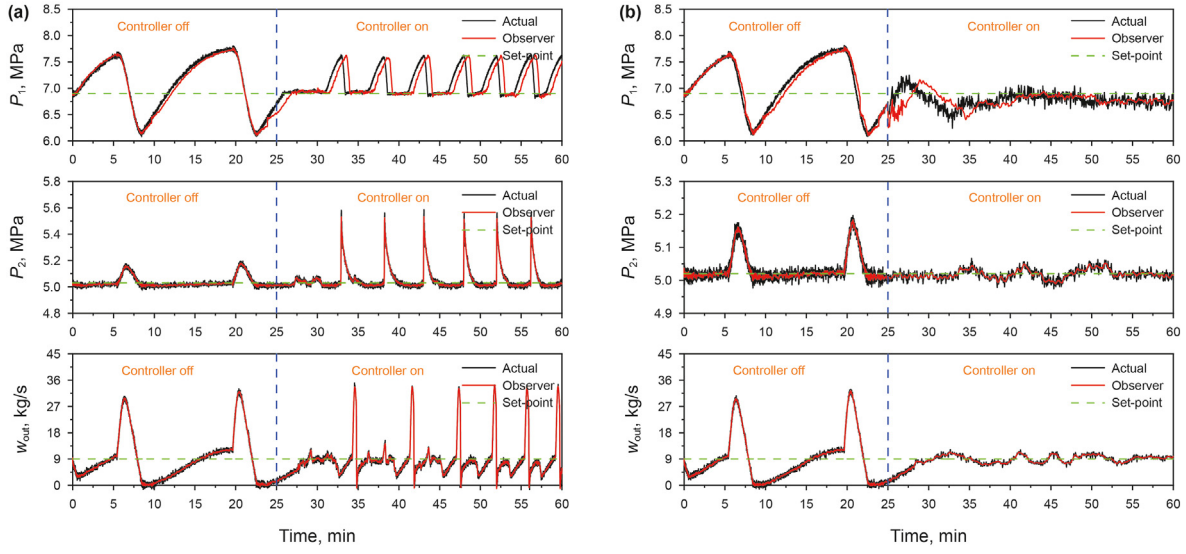

Fig. 14. Real-time control effect using different observers with 20% valve opening. (**a**) ODE-UKF as observer. (**b**) WNN-UKF as observer.

control performance is not ideal. To quantitatively compare the deviation between the actual value and the set-point in different control systems, we compare the integral squared error (ISE) and the integral absolute error (IAE), which are defined as follows:

$$\mathrm{ISE} = \int_0^t [e(t)]^2 \mathrm{d}t \tag{25}$$

$$\mathrm{IAE} = \int_0^t |e(t)| \mathrm{d}t \tag{26}$$

It can be seen from Table 4 that the overall error of WNN-UKF is smaller at the valve opening of 10% and 15%. This means that the uncertainty of the model is smaller, the response speed of the control system is faster, and the tracking performance is better. When the valve opening increases to 20%, as shown in Fig. 14, WNN-UKF stabilized the system successfully, but ODE-UKF failed. This is because the ODE model is linearly assumed. The transfer function in UKF is entirely static and cannot accurately capture real-time dynamic trends. The robustness of the closed-loop system is weak.

Besides modeling errors, the nonlinearity of the system is also the leading cause for robustness problems in severe slug flow control. Because WNN-UKF updates the nonlinear transfer function in the state equation at different times, the observer can provide accurate predictions to the controller. Therefore, it has excellent control performance with different valve openings. In the control process, the use of WNN requires fewer parameters and physical values, so after the controller is turned on, WNN-UKF has better control effect, faster stability of the system and more significant advantages in real-time control.

5. Conclusions and prospects

An observation method combining WNN and UKF is provided for severe slug flow control in this paper. In the proposed method, the subsea multiphase flow transportation is considered as a nonlinear model, and the modeling of the internal state of pipelines is realized by WNN, which can fully learn the dynamic characteristics of gas-liquid mixing. To accurately estimate the pipeline inlet pressure, WNN was introduced into the framework of UKF, forming a new observation method. It ensures the effective conversion of σ points in the time update phase and promotes the update of WNN simultaneously. Therefore, the transfer function in the UKF state equation will change with the update of the WNN after each update and can keep up with the changing trend of subsea pipeline pressure. The comparison results with ODE modeling show that WNN can better fit the relationship among top pressure, flow rate, valve opening and inlet pressure. The integration of the UKF algorithm can improve the system state estimation and provide more accurate estimation results for the controller to achieve real-time control. Compared with traditional methods, WNN-UKF offers better control and faster stabilization of the system. The valve opening can be up to 20%. The larger the valve opening, the higher the oil production rate. The simulation results verify the applicability and superiority of the method. The data-driven neural network enables the traditional filtering algorithm based on physical model to cope with nonlinear systems better. On the other hand, the real-time noise reduction ability of traditional filtering algorithm improves the generalization ability of neural networks obviously. The proposed WNN-UKF method has certain guiding significance for complementing their advantages. At the same time, WNN-UKF shows the possibility of the application of artificial intelligence method in the field of slug flow control, and provides a new idea for the practical application of future engineering.

Furthermore, the addition of neural networks and other methods can effectively improve the reliability of the control system and has certain guiding significance for oil and gas development under complex working conditions. For different working conditions, when using WNN-UKF, if the initial settings of parameters such as weights, scale scaling factors and time translation factors are not reasonable, the convergence speed of the whole network will become slow or even divergent. Therefore, the proper parameter selection is the difficulty of using this model. Moreover, when the amount of neural network training data is insufficient, the uncertainty of the model will increase. This will lead to the decrease of the initial prediction accuracy and the poor control effect of slug flow. Since neural networks rely heavily on data, they usually need to be retrained for different working conditions. Improving the adaptability of the neural network should be the focus of future work. Meanwhile it is necessary to study the constraint boundary of the controller.

Declaration of competing interest

The authors declare that they have no known competing financial interests or personal relationships that could have appeared to influence the work reported in this paper.

Acknowledgments

This work was supported by Development Project in Key Technical Field of Sichuan Province (2019ZDZX0030), International Science and Technology Innovation Cooperation Program of Sichuan Province (2021YFH0115) and Nanchong-SWPU Science and Technology Strategic Cooperation Project (SXHZ057) and Key and Core Technology Breakthrough Project of CNPC (2021ZG08).

Appendix A. ODE model details

The model was proposed by Jahanshahi and Skogestad (2011), and the specific details are as follows:

(1) Inflow conditions

The inlet boundary conditions usually change. The liquid volume fraction in the pipeline section can be obtained based on the liquid mass fraction and densities of the two-phase:

$$\alpha_{\mathrm{L}} = \frac{\alpha_{\mathrm{Lm}}/\rho_{\mathrm{L}}}{\alpha_{\mathrm{Lm}}/\rho_{\mathrm{L}} + (1-\alpha_{\mathrm{Lm}})/\rho_{\mathrm{G}}} \tag{27}$$

The average liquid mass fraction in the pipeline section can be attained using the inflow boundary condition:

$$\overline{\alpha}_{\mathrm{Lm1}} \cong \frac{w_{\mathrm{L,in}}}{w_{\mathrm{G,in}} + w_{\mathrm{L,in}}} \tag{28}$$

Combing the two above equations gives the average liquid volume fraction in the pipeline:

$$\overline{\alpha}_{\mathrm{L1}} \cong \frac{\overline{\rho}_{\mathrm{G1}} w_{\mathrm{L,in}}}{\overline{\rho}_{\mathrm{G1}} w_{\mathrm{L,in}} + \rho_{\mathrm{L}} w_{\mathrm{G,in}}} \tag{29}$$

In Eq. (29), the gas density can be calculated based on the nominal pressure (steady-state) of the pipeline:

$$\overline{\rho}_{G1}=\frac{P_{1,nom}M_G}{RT_1} \tag{30}$$

(2) Outflow conditions

After the long transport pipeline reaches the offshore platform, its external boundary pressure is constant (separator pressure). The constant pressure condition and the choke valve model are used as the boundary conditions at the outlet of the riser.

$$w_{mix,out}=C_{k3}f(z)\sqrt{\rho_t(P_2-P_0)} \tag{31}$$

where $z\in(0,1)$ and $f(z)$ is the equation for the opening of the valve. A linear valve is assumed in the simulation model (i.e., $f(z)=z$).

The equation of gas and liquid outflow is.

$$w_{L,out}=\alpha_{Lm,t}w_{mix,out} \tag{32}$$

$$w_{G,out}=(1-\alpha_{Lm,t})w_{mix,out} \tag{33}$$

To calculate the mass flow rate of each phase in the outlet model in Eqs. (32) and (33), also the mixing density ρ_t, used in Eq. (31), the phase distribution at the top of the riser must be known.

The liquid mass fraction at the outlet choke valve:

$$w_{G,out}=(1-\alpha_{Lm,t})w_{mix,out} \tag{34}$$

$$\alpha_{Lm,t}=\frac{\alpha_{L,t}\rho_L}{\alpha_{L,t}\rho_L+(1-\alpha_{L,t})\rho_{G2}} \tag{35}$$

The density of the two-phase mixture at the top of the riser:

$$\rho_t=\alpha_{L,t}\rho_L+(1-\alpha_{L,t})\rho_{G2} \tag{36}$$

The above equation $\alpha_{L,t}$ is the liquid volume fraction at the top of the riser. The pressure and liquid volume fraction between the vertical gravity-dominated two-phase flow pipes are approximately linear for the desired steady flow state. The pressure gradient along the riser can be assumed to be constant. Due to the assumed linear relationship, the liquid volume fraction also maintains an approximately constant gradient along the riser for a steady flow state.

$$\frac{\partial\alpha_{L2}}{\partial y}=\text{constant} \tag{37}$$

This assumption indicates that the volume fraction of the liquid in the middle of the riser is the average of the volume fractions at both ends of the riser. On the other hand, the volume fraction of liquid in the middle of the riser is approximately equal to the average volume fraction of liquid in the riser. Therefore,

$$\overline{\alpha}_{L2}=\frac{\alpha_{L,lp}+\alpha_{L,t}}{2} \tag{38}$$

The liquid volume fraction $\alpha_{L,lp}$ at the bottom of the riser is determined by the flow area of the liquid phase at the low point.

$$\alpha_{L,t}=2\overline{\alpha}_{L2}-\alpha_{L,lp}=\frac{2m_{L2}}{V_2\rho_L}-\frac{A_L}{\pi r_1^2} \tag{39}$$

(3) Pipeline model

In the pipeline, the gas and liquid are usually distributed unevenly. In this case, the mass of the liquid in the pipeline is given by $\overline{m}_{L1}=\rho_L V_1\overline{\alpha}_{L1}$. The lowest point of the pipeline level at the bottom of the riser can be defined as $\overline{h}_1\cong h_c\overline{\alpha}_{L1}$. If the mass of the liquid in the pipeline increases, the level at the bottom of the riser will also change, and its position changes have the following relationship.

$$\begin{aligned}\Delta h_1&=\Delta L\sin(\theta)\\ \Delta m_{L1}&=\Delta L\pi r_1^2(1-\overline{\alpha}_{L1})\rho_L\\ h_1&=\overline{h}_1+\Delta L\sin(\theta)\\ h_1&=\overline{h}_1+\frac{\Delta m_{L1}}{\pi r_1^2(1-\overline{\alpha}_{L1})\rho_L}\sin(\theta)\\ \overline{h}_1&=K_h h_c\overline{\alpha}_{L1}\end{aligned} \tag{40}$$

where K_h is the correction factor around unity which can be used for fine-tuning of the model.

Therefore, the liquid level of h_1 in the pipeline can be expressed as a function of the liquid mass m_{L1} in the pipe. The functional relationship can be expressed as:

$$h_1=K_h\overline{h}_1+\left(\frac{m_{L1}-\rho_{L,r}V_1\overline{\alpha}_{L1}}{\pi r_1^2(1-\overline{\alpha}_{L1})\rho_L}\right)\sin(\theta) \tag{41}$$

where m_{L1} is the state variable of the model. The remaining parameters are constant.

The volume occupied by the gas in the pipe:

$$V_{G1}=V_1-\frac{(1-\alpha_{L,t})m_{L1}}{\rho_{L,r}} \tag{42}$$

Gas density in the pipeline:

$$\rho_{G1}=\frac{m_{G1}}{V_{G1}} \tag{43}$$

Pressure in pipeline assuming ideal gas:

$$P_1=\frac{\rho_{G1}RT_1}{M_G} \tag{44}$$

For the pressure loss due to friction in the pipeline, only the friction of the liquid is considered.

$$\Delta P_{fp}=\frac{\overline{\alpha}_{L1}\lambda_p\rho_L\overline{U}_{sl,in}^2L_1}{4r_1} \tag{45}$$

The correlation for turbulence flow in smooth wall pipes is used as the friction factor in the pipeline.

$$\lambda_p=0.0056+0.5Re_p^{-0.32} \tag{46}$$

Reynolds number in the pipeline:

$$Re_p=\frac{2\rho_L\overline{U}_{sl,in}r_1}{\mu} \tag{47}$$

where μ is the liquid viscosity and $U_{sl,in}$ is the surface velocity of the inlet liquid:

$$\overline{U}_{sl,in}=\frac{w_{L,in}}{\pi r_1^2\rho_L} \tag{48}$$

(4) Riser model

The total volume of riser:

$$V_2 = \pi r_2^2 (L_2 + L_3) \tag{49}$$

The volume occupied by gas in the riser:

$$V_{G2} = V_2 - \frac{m_{L2}}{\rho_L} \tag{50}$$

The density of gas at the top of the riser:

$$\rho_{G2} = \frac{m_{G2}}{V_{G2}} \tag{51}$$

Pressure at the top of the riser:

$$P_2 = \frac{\rho_{G2} R T_2}{M_G} \tag{52}$$

Average liquid volume fraction in riser:

$$\overline{\alpha}_{L2} = \frac{m_{L2}}{V_2 \rho_L} \tag{53}$$

The average density of mixture inside riser:

$$\overline{\rho}_m = \frac{m_{G2} + m_{L2}}{V_2} \tag{54}$$

Friction loss in the riser:

$$\Delta P_{fr} = \frac{\overline{\alpha}_{L2} \lambda_r \overline{\rho}_m \overline{U}_m^2 (L_2 + L_3)}{4 r_2} \tag{55}$$

The friction factor of riser using the same correlation as a pipeline:

$$\lambda_r = 0.0056 + 0.5 Re_r^{-0.32} \tag{56}$$

Reynolds number of flow in riser:

$$Re_r = \frac{2 \overline{\rho}_m \overline{U}_m r_2}{\mu} \tag{57}$$

Riser fluid mixing speed:

$$\overline{U}_m = \overline{U}_{sl2} + \overline{U}_{sg2} \tag{58}$$

Among them:

$$\begin{aligned} \overline{U}_{sl2} &= \frac{w_{L,in}}{\rho_L \pi r_2^2} \\ \overline{U}_{sg2} &= \frac{w_{G,in}}{\rho_{G2} \pi r_2^2} \end{aligned} \tag{59}$$

(5) Gas flow model at the bottom of the riser.

When the liquid height at the bottom of the riser exceeds the critical level($h_1 \geq h_c$), slugging will occur at the bottom of the riser and the gas flow rate is zero.

$$w_{G,lp} = 0, h_1 \geq h_c \tag{60}$$

When the liquid is not blocked at the bottom of the riser($h_1 < h_c$), the gas will flow from volume V_{G1} to V_{G2} with a mass flow rate of $w_{G,lp}$. According to the physical model, the two most important parameters determining the gas rate are the pressure drop over the low-point and the opening area. This suggests that the flow of gas can be approximated by a valve flow model. The pressure drop drives the gas through an opening area of A_G.

$$w_{G,lp} = K_G A_G \sqrt{\rho_{G1} \Delta P_G}, h_1 < h_c \tag{61}$$

Among them:

$$\Delta P_G = P_1 - \Delta P_{fp} - P_2 - \overline{\rho}_m g L_2 - \Delta P_{fr} \tag{62}$$

(6) Liquid flow model at the bottom of the riser.

The liquid at the bottom of the riser can also be used similarly to the equation for the gas at the bottom of the riser.

$$w_{L,lp} = K_L A_L \sqrt{\rho_L \Delta P_L} \tag{63}$$

Among them:

$$\Delta P_L = P_1 - \Delta P_{fp} + \rho_L g h_1 - P_2 - \overline{\rho}_m g L_2 - \Delta P_{fr} \tag{64}$$

The area of the gas flow is calculated exactly using some trigonometric functions. For simplicity, a quadratic approximation is used in the proposed model.

$$A_G \cong \pi r_1^2 \left(\frac{h_c - h_1}{h_c} \right)^2, h_1 < h_c \tag{65}$$

$$A_L = \pi r_1^2 - A_G \tag{66}$$

References

Aamo, O.M., Eikrem, G.O., Siahaan, H.B., Foss, B.A., 2005. Observer design for multiphase flow in vertical pipes with gas-lift––theory and experiments. J. Process Control 15 (3), 247–257. https://doi.org/10.1016/j.jprocont.2004.07.002.

Abiyev, R.H., Kaynak, O., Kayacan, E., 2013. A type-2 fuzzy wavelet neural network for system identification and control. J. Franklin Inst. 350 (7), 1658–1685. https://doi.org/10.1016/j.jfranklin.2013.04.020.

Arulampalam, M.S., Maskell, S., Gordon, N., Clapp, T., 2002. A tutorial on particle filters for online nonlinear/non-Gaussian Bayesian tracking. IEEE Trans. Signal Process. 50 (2), 174–188. https://doi.org/10.1109/78.978374.

Backi, C.J., Grimes, B.A., Skogestad, S., 2018. A control- and estimation-oriented gravity separator model for oil and gas applications based upon first-principles. Ind. Eng. Chem. Res. 57 (21), 7201–7217. https://doi.org/10.1021/acs.iecr.7b04297.

Bendlksen, K.H., Malnes, D., Moe, R., Nuland, S., 1991. The dynamic two-fluid model OLGA: theory and application. SPE Prod. Eng. 6 (2), 171–180. https://doi.org/10.2118/19451-PA.

Di Meglio, F., Petit, N., Alstad, V., Kaasa, G.O., 2012. Stabilization of slugging in oil production facilities with or without upstream pressure sensors. J. Process Control 22 (4), 809–822. https://doi.org/10.1016/j.jprocont.2012.02.014.

Duan, F., Dai, L.L., Chang, W.N., Chen, Z.Q., Zhu, C., Li, W., 2016. sEMG-based identification of hand motion commands using wavelet neural network combined with discrete wavelet transform. IEEE Trans. Ind. Electron. 63 (3), 1923–1934. https://doi.org/10.1109/TIE.2015.2497212.

Ehinmowo, A.B., Cao, Y., 2016. Stability analysis of slug flow control. Systems Science & Control Engineering 4 (1), 183–191. https://doi.org/10.1080/21642583.2016.1213189.

Forootan, M.M., Larki, I., Zahedi, R., Ahmadi, A., 2022. Machine learning and deep learning in energy systems: a review. Sustainability 14 (8), 1–49. https://doi.org/10.3390/su14084832.

Godhavn, J.-M., Fard, M.P., Fuchs, P.H., 2005. New slug control strategies, tuning rules and experimental results. J. Process Control 15 (5), 547–557. https://doi.org/10.1016/j.jprocont.2004.10.003.

Guo, T., Zhang, T., Lim, E., López-Benítez, M., Ma, F., Yu, L., 2022. A review of wavelet analysis and its applications: challenges and opportunities. IEEE Access 10, 58869–58903. https://doi.org/10.1109/ACCESS.2022.3179517.

Havre, K., Stornes, K.O., Stray, H., 2001. Taming slug flow in pipelines. Pipes Pipelines

Int. 46 (2), 23–31.
Jahanshahi, E., Backi, C.J., Skogestad, S., 2017. Anti-slug control based on a virtual flow measurement. Flow Meas. Instrum. 53, 299–307. https://doi.org/10.1016/j.flowmeasinst.2017.01.008.
Jahanshahi, E., Skogestad, S., 2011. Simplified dynamical models for control of severe slugging in multiphase risers. IFAC Proc. Vol. 44 (1), 1634–1639. https://doi.org/10.3182/20110828-6-IT-1002.00981.
Jahanshahi, E., Skogestad, S., 2017. Nonlinear control solutions to prevent slugging flow in offshore oil production. J. Process Control 54, 138–151. https://doi.org/10.1016/j.jprocont.2017.03.014.
Jahanshahi, E., Skogestad, S., Grøtli, E.I., 2013a. Anti-slug control experiments using nonlinear observers. In: 2013 American Control Conference. Washington, DC, USA. https://doi.org/10.1109/ACC.2013.6579976.
Jahanshahi, E., Skogestad, S., Grøtli, E.I., 2013b. Nonlinear model-based control of two-phase flow in risers by feedback linearization. IFAC Proc. Vol. 46 (23), 301–306. https://doi.org/10.3182/20130904-3-FR-2041.00041.
Jahanshahi, E., Skogestad, S., Helgesen, A.H., 2012. Controllability analysis of severe slugging in well-pipeline-riser systems. IFAC Proc. Vol. 45 (8), 101–108. https://doi.org/10.3182/20120531-2-NO-4020.00014.
Julier, S.J., 2004. Unscented filtering and nonlinear estimation. Proc. IEEE 92 (3), 401–422. https://doi.org/10.1109/JPROC.2003.823141.
Julier, S.J., Uhlmann, J.K., 1997. A non-divergent estimation algorithm in the presence of unknown correlations. In: Proceedings of the 1997 American Control Conference (Cat. No.97CH36041). Albuquerque, NM, USA.
Kaczmarek, M., 2016. Comparison of estimation accuracy of EKF, UKF and PF filters. Annu. Navig. 23 (1), 69–87. https://doi.org/10.1515/aon-2016-0005.
Lei, Y., Yang, B., Jiang, X., Jia, F., Li, N., Nandi, A.K., 2020. Applications of machine learning to machine fault diagnosis: a review and roadmap. Mech. Syst. Signal Process. 138, 106587. https://doi.org/10.1016/j.ymssp.2019.106587.
Lin, J., de Weck, O., de Neufville, R., Yue, H.K., 2013. Enhancing the value of offshore developments with flexible subsea tiebacks. J. Petrol. Sci. Eng. 102, 73–83. https://doi.org/10.1016/j.petrol.2013.01.003.
Mao, J., Yang, J., Gong, J., 2016. Liuhua19-5 gas field development: a successful subsea tie back solution. In: The 26th International Ocean and Polar Engineering Conference. Rhodes, Greece.
Meglio, F.D., Kaasa, G.O., Petit, N., 2009. A first principle model for multiphase slugging flow in vertical risers. Shanghai,China. In: Proceedings of the 48h IEEE Conference on Decision and Control (CDC) Held Jointly with 2009 28th Chinese Control Conference. https://doi.org/10.1109/CDC.2009.5400680.
Oliveira, V.d., Jäschke, J., Skogestad, S., 2015. An autonomous approach for driving systems towards their limit: an intelligent adaptive anti-slug control system for production maximization. IFAC-PapersOnLine 48 (6), 104–111. https://doi.org/10.1016/j.ifacol.2015.08.017.
Rajankar, S.O., Talbar, S.N., 2015. An optimum ECG denoising with wavelet neural network. In: 2015 International Conference on Pervasive Computing (ICPC). Pune, India. https://doi.org/10.1109/PERVASIVE.2015.7087204.
Ramadevi, B., Bingi, K., 2022. Chaotic time series forecasting approaches using machine learning techniques: a review. Symmetry-Basel 14 (5), 955. https://doi.org/10.3390/sym14050955.
Sivertsen, H., Alstad, V., Skogestad, S., 2009. Medium-scale experiments on stabilizing riser-slug flow. SPE Proj. Facil. Constr. 4 (4), 156–170. https://doi.org/10.2118/120040-PA.
Skofteland, G., Godhavn, J.-M., 2003. Suppression of slugs in multiphase flow lines by active use of topside choke - field experience and experimental results. In: 11th International Conference on MULTIPHASE 03: Extending the Boundaries of Flow Assurance. San Remo, Italy.
Storkaas, E., Skogestad, S., 2004. Cascade control of unstable systems with application to stabilization of slug flow. IFAC Proc. Vol. 37 (1), 335–340. https://doi.org/10.1016/S1474-6670(17)38754-2.
Storkaas, E., Skogestad, S., 2007. Controllability analysis of two-phase pipeline-riser systems at riser slugging conditions. Control Eng. Pract. 15 (5), 567–581. https://doi.org/10.1016/j.conengprac.2006.10.007.
Storkaas, E., Skogestad, S., Godhavn, J.M., 2003. A low-dimensional dynamic model of severe slugging for control design and analysis. In: 11th International Conference on MULTIPHASE 03: Extending the Boundaries of Flow Assurance. San Remo, Italy.
Syre, T.V., 2012. Anti-Slug Control with Non-linear State Estimation. Norges teknisk-naturvitenskapelige universitet, Fakultet for informasjonsteknologi.
Taitel, Y., Dukler, A.E., 1977. A model for slug frequency during gas-liquid flow in horizontal and near horizontal pipes. Int. J. Multiphas. Flow 3 (6), 585–596. https://doi.org/10.1016/0301-9322(77)90031-3.
Xia, X., Liu, X.F., Lou, J.C., 2020. A network traffic prediction model of smart substation based on IGSA-WNN. ETRI J. 42 (3), 366–375. https://doi.org/10.4218/etrij.2019-0040.
Xiao, J.J., Shonham, O., Brill, J.P., 1990. A comprehensive mechanistic model for two-phase flow in pipelines. In: SPE Annual Technical Conference and Exhibition. https://doi.org/10.2118/20631-MS.
Xin, W., Jiayi, W., Xin, L., 2018. A feed-forward wavelet neural network adaptive observer-based fault detection technique for spacecraft attitude control systems. Chin. J. Electron. 27 (1), 102–108. https://doi.org/10.1049/cje.2017.11.010.
Zhao, R., Yan, R., Chen, Z., Mao, K., Wang, P., Gao, R.X., 2019. Deep learning and its applications to machine health monitoring. Mech. Syst. Signal Process. 115, 213–237. https://doi.org/10.1016/j.ymssp.2018.05.050.